# Paxillin phosphorylation at Ser273 localizes a GIT1–PIX–PAK complex and regulates adhesion and protrusion dynamics

Anjana Nayal,[1] Donna J. Webb,[2] Claire M. Brown,[3] Erik M. Schaefer,[4] Miguel Vicente-Manzanares,[1] and Alan Rick Horwitz[1]

[1]Department of Cell Biology, University of Virginia, Charlottesville, VA 22908
[2]Department of Biological Sciences and Vanderbilt Kennedy Center for Research on Human Development, Vanderbilt University, Nashville, TN 37235
[3]Life Sciences Complex Imaging Facility, Department of Physiology, McGill University, Montreal, Quebec, H3G 1Y6, Canada
[4]BioSource International, Hopkinton, MA 01748

Continuous adhesion formation and disassembly (adhesion turnover) in the protrusions of migrating cells is regulated by unclear mechanisms. We show that p21-activated kinase (PAK)–induced phosphorylation of serine 273 in paxillin is a critical regulator of this turnover. Paxillin-S273 phosphorylation dramatically increases migration, protrusion, and adhesion turnover by increasing paxillin–GIT1 binding and promoting the localization of a GIT1–PIX–PAK signaling module near the leading edge. Mutants that interfere with the formation of this ternary module abrogate the effects of paxillin-S273 phosphorylation. PAK-dependent paxillin-S273 phosphorylation functions in a positive-feedback loop, as active PAK, active Rac, and myosin II activity are all downstream effectors of this turnover pathway. Finally, our studies led us to identify in highly motile cells a class of small adhesions that reside near the leading edge, turnover in 20–30 s, and resemble those seen with paxillin-S273 phosphorylation. These adhesions appear to be regulated by the GIT1–PIX–PAK module near the leading edge.

## Introduction

Cell migration is a spatiotemporally regulated process marked by the formation and disassembly of adhesions, which are complex supramolecular structures that connect the extracellular matrix to actin (Schoenwaelder and Burridge, 1999). In the front of migrating cells, the continuous formation and disassembly of adhesions (adhesion turnover) is highly regulated and appears to be coupled to protrusion formation (Webb et al., 2004). Although several regulators of adhesion turnover, including paxillin (Webb et al., 2004), G protein–coupled receptor kinase–interacting protein 1 (GIT1; Zhao et al., 2000), FAK (Ren et al., 2000), Src (Webb et al., 2004), and p21-activated kinase (PAK; Manser et al., 1997) are known, how these molecules act together to regulate adhesion turnover is not clear.

Correspondence to Alan Rick Horwitz: horwitz@virginia.edu

Abbreviations used in this paper: CA, constitutively active; DIC, differential interference contrast; IRM, interference reflection microscopy; GEF, guanine nucleotide exchange factor; GIT, G protein–coupled receptor kinase–interacting protein; KD, kinase-dead; MEF, mouse embryonic fibroblast; MLC, myosin light chain; PAK, p21-activated kinase; PBD, p21 binding domain; PIX, PAK-interactive exchange factor; seCFP, super-enhanced cyan fluorescent protein; SHD, Spa2 homology domain; TIRF, total internal reflection fluorescence; WT, wild-type.

The online version of this article contains supplemental material.

Paxillin is a key regulator of adhesion turnover, as it interacts with several adhesion proteins (Brown and Turner, 2004) through its five $NH_2$-terminal LD domains, four COOH-terminal LIM domains, and multiple SH3 and SH2 binding domains (Turner, 2000). The LD4 domain of paxillin binds FAK and GIT1 (Brown and Turner, 2004) and is implicated in adhesion turnover (Zhao et al., 2000; Webb et al., 2004). Paxillin targets GIT1 to the leading edge and adhesions (Manabe et al., 2002), and GIT1 overexpression sequesters paxillin from adhesions (Zhao et al., 2000), implicating this interaction in adhesion disassembly. Cells expressing an LD4-deletion paxillin mutant show perturbed migration and protrusion (West et al., 2001). Also, GIT1 is a key regulator of protrusion (Manabe et al., 2002), raising the possibility that the paxillin–GIT1 interaction may regulate and thus link adhesion turnover and protrusion formation.

GIT1, through its Spa2 homology domain (SHD), binds to the Rac exchange factor PAK-interactive exchange factor (PIX), which in turn binds the Rac effector PAK (Manser et al., 1998), forming a trimolecular GIT1–PIX–PAK signaling complex (Manabe et al., 2002). GIT1 functions in part by targeting PIX and PAK to different subcellular zones (e.g., adhesions and the leading edge) in fibroblasts and epithelial cells (Manabe et al., 2002).


The Journal of Cell Biology, Vol. 173, No. 4, May 22, 2006 587–599
http://www.jcb.org/cgi/doi/10.1083/jcb.200509075

This module is also implicated in neuronal synapse formation (Zhang et al., 2005) and immunological synapse organization through local Rac and PAK activation (Phee et al., 2005). PAK is also implicated in adhesion stability (Zhao et al., 2000) through its kinase activity (Manser et al., 1997), and the PIX–PAK complex is required for protrusion formation (Cau and Hall, 2005).

Phosphorylation is a likely mechanism by which paxillin–GIT1 binding is regulated, as it regulates the interaction of paxillin with other binding partners (Liu et al., 2002; Ishibe et al., 2003). We recently identified a novel phosphorylation site at serine residue 273 in paxillin (S273-paxillin; Webb et al., 2005) that resides in its LD4 domain and thus can potentially regulate paxillin–GIT1 binding. We show that S273-paxillin phosphorylation is PAK-mediated and up-regulates adhesion turnover and protrusion by increasing paxillin–GIT1 binding and Rac activation. It also targets the components of the GIT1–PIX–PAK module near the leading edge to a population of small and highly dynamic adhesions. These adhesions exhibit very fast turnover and differ substantially in size and location from the adhesions studied earlier. Also, PAK activation is required for faster adhesion turnover and protrusion dynamics downstream of S273-paxillin phosphorylation through myosin. Collectively, we demonstrate a novel positive-feedback mechanism that regulates and couples adhesion and protrusion dynamics through the localization of a pax–GIT1–PIX–PAK complex.

## Results

### PAK-mediated phosphorylation of paxillin at S273 regulates its interaction with GIT1

We recently used mass spectrometry to identify several utilized phosphorylation sites on paxillin (Webb et al., 2005). Of these, S273 lies within the LD4 domain, and therefore its phosphorylation could regulate paxillin binding to FAK or GIT1. To determine whether S273-paxillin phosphorylation occurs in CHO-K1 cells, we assessed S273-paxillin phosphorylation in lysates prepared from CHO-K1 cells plated under migration-promoting conditions (see Materials and methods) by immunoblotting using a phospho–S273-paxillin–specific antibody that recognized phosphomimetic S273D-paxillin but not nonphosphorylatable S273A-paxillin (Fig. S1 a, available at http://www.jcb.org/cgi/content/full/jcb.200509075/DC1). Phospho–S273-paxillin antibody specificity was confirmed by phosphopeptide competition (Fig. S1 b). We observed a single band corresponding to the molecular mass of paxillin (~68 kD) in lysates treated with CalyculinA (a Ser/Thr phosphatase inhibitor), with no detectable

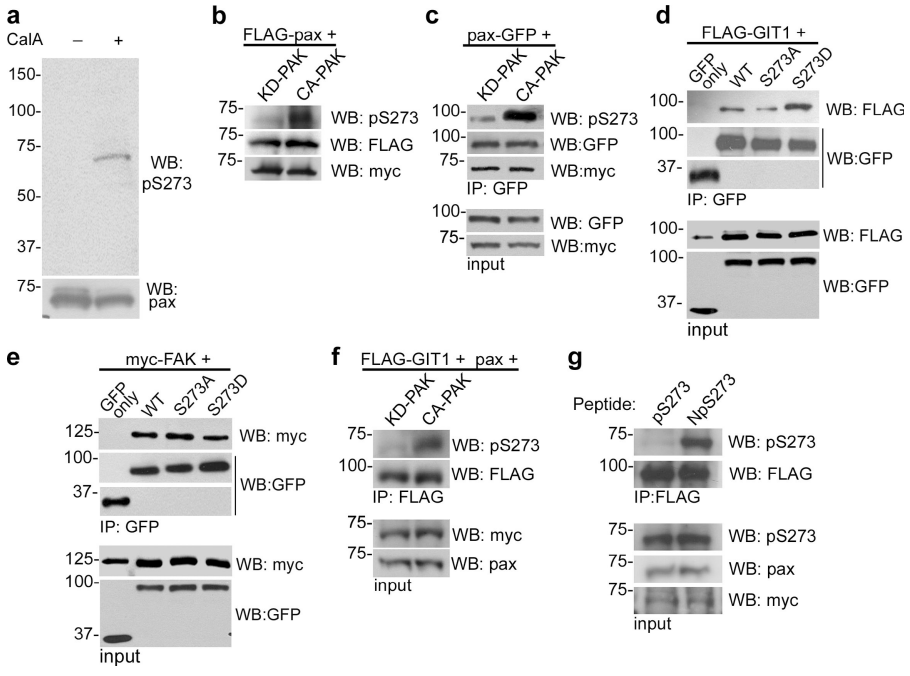


Figure 1. **S273-paxillin phosphorylation by PAK regulates paxillin–GIT1 binding.** (a) CHO-K1 lysates treated (right) and untreated (left) with 5 nM CalyculinA (CalA) were probed (top) using a phospho–S273-paxillin–specific antibody. Total paxillin levels were assayed with an anti-paxillin antibody (bottom). A single band corresponding to the molecular mass of paxillin (~68 kD) was detected in treated lysates. (b) Kinase assay was performed with FLAG-WT-paxillin and either KD- or CA-myc-PAK synthesized in vitro, and S273-paxillin phosphorylation was assessed with a phospho–S273-paxillin antibody. Bottom blots show equal loading by probing with anti-FLAG and anti-myc antibodies, respectively. Phospho–S273-paxillin levels increased eightfold with CA-PAK compared with KD-PAK. (c) Paxillin was immunoprecipitated using a GFP antibody from CHO-K1 lysates expressing paxillin-GFP and either KD- or CA-myc-PAK, and S273-paxillin phosphorylation levels were assayed using a phospho–S273-paxillin antibody. The lower two panels show equal levels of paxillin–GFP and myc-PAK, and the GFP blot shows equal loading in the lysates. S273-paxillin phosphorylation increased eightfold with CA-PAK as compared with KD-PAK. (d) A GFP antibody was used to immunoprecipitate paxillin from CHO-K1 lysates expressing GFP control or WT-, S273A-, or S273D-paxillin-GFP and FLAG-GIT1. GIT1 binding was probed using an anti-FLAG antibody. The bottom two panels show equivalent expression of S273-paxillin mutants and FLAG-GIT1 in the lysates. GIT1 binding to S273D-paxillin increased threefold, whereas it was reduced twofold with S273A-paxillin, when compared with WT-paxillin. (e) Paxillin was immunoprecipitated from CHO-K1 lysates expressing GFP control or WT-, S273A-, or S273D-paxillin-GFP and myc-FAK using a GFP antibody, and FAK binding was assessed with an anti-myc antibody. The bottom two panels show equivalent expression of S273-paxillin mutants and myc-FAK in the lysates. S273-paxillin phosphorylation only marginally affected FAK binding. (f) GIT1 was immunoprecipitated from in vitro mixtures of FLAG-GIT1, untagged WT-paxillin, and either KD- or CA-PAK using anti-FLAG M2-conjugated agarose, and phospho–S273-paxillin binding was probed using a phospho–S273-paxillin antibody. The middle blot shows equal levels of FLAG-GIT1 using an anti-FLAG antibody. (bottom) Equal loading of the lysates using anti-myc and anti-paxillin antibodies, respectively. Phospho–S273-paxillin–GIT1 binding increased sevenfold with CA-PAK compared with KD-PAK. (g) Anti-FLAG M2-conjugated agarose was used to immunoprecipitate GIT1 from in vitro mixtures of FLAG-GIT1, untagged WT-paxillin, and CA-PAK preincubated with 500-fold molar excess of phospho– or nonphospho–S273-paxillin peptide, and phospho–S273-paxillin binding was assessed with a phospho–S273-paxillin antibody. Very low levels of phospho–S273-paxillin–GIT1 binding was detected with the competitive phosphopeptide (left), whereas a robust signal was observed with the noncompetitive peptide (right), confirming that the PAK-mediated increase in phospho–S273-paxillin–GIT1 binding is specific to S273-paxillin phosphorylation.

signal in untreated lysates (Fig. 1 a), suggesting that S273-paxillin is a labile phosphorylation site. During cell spreading, S273-paxillin phosphorylation was detected at low levels in suspended cells with an increase after 1 h of spreading until 3.5 h (Fig. S1, c and d).

Paxillin is a substrate of PAK (Hashimoto et al., 2001), and the LD4 domain (N-LDELMAS*L-C) has a glutamic acid residue four residues upstream of S273; from peptide studies, this is a favored recognition determinant for PAK (Tuazon et al., 1997). To determine whether S273-paxillin is phosphorylated by PAK, we performed a kinase assay with in vitro–synthesized FLAG-paxillin and either myc-tagged, kinase-dead (KD), or constitutively active (CA) PAK and assayed phospho–S273-paxillin levels by immunoblotting using the phospho–S273-paxillin antibody. Equal loading was confirmed by immunoblotting with anti-FLAG or anti-myc antibodies. Low levels of phospho–S273-paxillin were detected with KD-PAK, whereas a robust signal (eightfold increase) was observed with CA-PAK (Fig. 1 b). We also observed a similar eightfold increase in S273-paxillin phosphorylation when paxillin-GFP was immunoprecipitated from CHO-K1 cells coexpressing wild-type (WT)–paxillin-GFP and KD- or CA-myc-PAK (Fig. 1 c).

Next, we assayed the binding of the S273-paxillin mutants with FAK and GIT1. Paxillin was immunoprecipitated from CHO-K1 cells coexpressing either WT-, S273D-, or S273A-paxillin-GFP and FLAG-GIT1 or myc-FAK. Similar levels of expression for paxillin-GFP and FLAG-GIT1 or myc-FAK were confirmed from immunoblots of the lysates (Fig. 1, d and e). GIT1 or FAK binding was assessed by immunoblotting. GIT1 binding to S273D-paxillin increased about threefold, whereas it decreased twofold with S273A-paxillin, compared with WT-paxillin (Fig. 1 d). In contrast, FAK binding changed modestly, if any, increasing by 25.0 ± 8.0% ($P < 0.05$) with S273A-paxillin and decreasing to 73.0 ± 3.0% ($P < 0.01$) with S273D-paxillin, compared with WT-paxillin (Fig. 1 e). To confirm the differential binding of phospho–S273-paxillin to GIT1, using an in vitro expression system, we synthesized FLAG-GIT1, untagged WT-paxillin, and myc-tagged KD- or CA-PAK. We then immunoprecipitated GIT1 and assessed the amount of phospho–S273-paxillin bound to GIT1 by immunoblotting. There was a sevenfold increase in the level of phospho–S273-paxillin bound to FLAG-GIT1 in the presence of CA-versus KD-PAK (Fig. 1 f). Similar results were obtained when we probed using an anti-paxillin antibody (unpublished data). This effect was specific because incubation with a phospho–S273-paxillin peptide abolished phospho–S273-paxillin–GIT1 binding, whereas the nonphospho–S273-paxillin peptide had no effect (Fig. 1 g). Together, our data demonstrate that S273-paxillin phosphorylation is directly mediated by PAK and regulates binding of paxillin to GIT1.

## S273-paxillin phosphorylation increases cell migration and protrusive activity

The functional significance of S273-paxillin phosphorylation was determined by assaying its effects on cell migration. The migration rates for S273A-paxillin–expressing CHO-K1 cells showed a >40% decrease (20.0 ± 2.0 μm/h; $n = 30$), whereas they increased by nearly 30% (45.0 ± 3.0 μm/h; $n = 30$; $P < 0.01$) for S273D-paxillin, compared with WT-paxillin (35.0 ± 3.0 μm/h; $n = 30$; $P < 0.0001$). Fig. 2 a shows the individual cell tracks of CHO-K1 cells expressing WT-, S273A-, or S273D-paxillin transposed to a common origin. When compared with

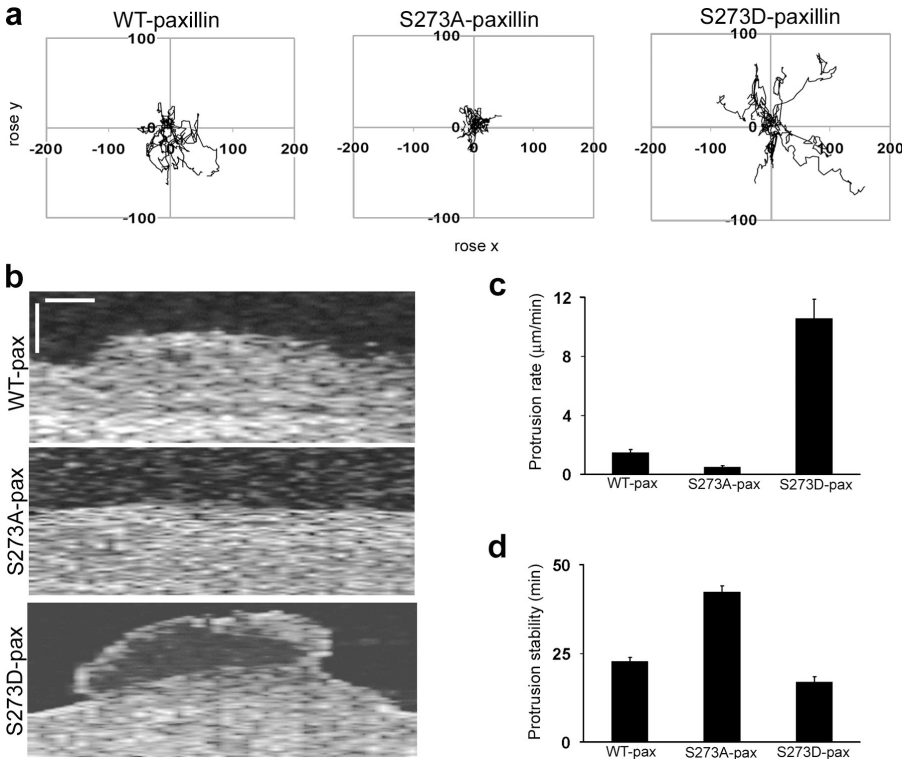


Figure 2. **S273-paxillin phosphorylation increases cell migration and protrusiveness.** (a) Wind rose plots for CHO-K1 cells expressing WT-, S273A- or S273D-paxillin-GFP. S273A-paxillin expression led to shorter migration paths (middle), whereas those for S273D-paxillin were significantly longer (right) compared with WT-paxillin (left). The plots show data from nine representative cells from three independent experiments. (b) Kymographs from CHO-K1 cells expressing WT-, S273A-, or S273D-paxillin-GFP. Cell edges were enhanced using the Sobel algorithm in the Fluoview software. Cells expressing S273D-paxillin-GFP show rapid membrane extension and retraction (bottom) when compared with cells expressing S273A-paxillin-GFP (middle). WT-paxillin-GFP–expressing cells show intermediate membrane activity (top). Bars: (vertical) 5 μm; (horizontal) 5 min. (c) Quantification of protrusion rates from kymographs. S273D-paxillin mutant increases, whereas S273A-paxillin reduces the protrusion rate with respect to WT-paxillin. (d) Protrusion stability in S273D-paxillin–expressing cells decreased, whereas it increased in S273A-paxillin–expressing cells. A minimum of eight cells and at least three protrusions per cell from three independent experiments were analyzed for each kymograph analysis. Error bars represent SEM from three experiments.

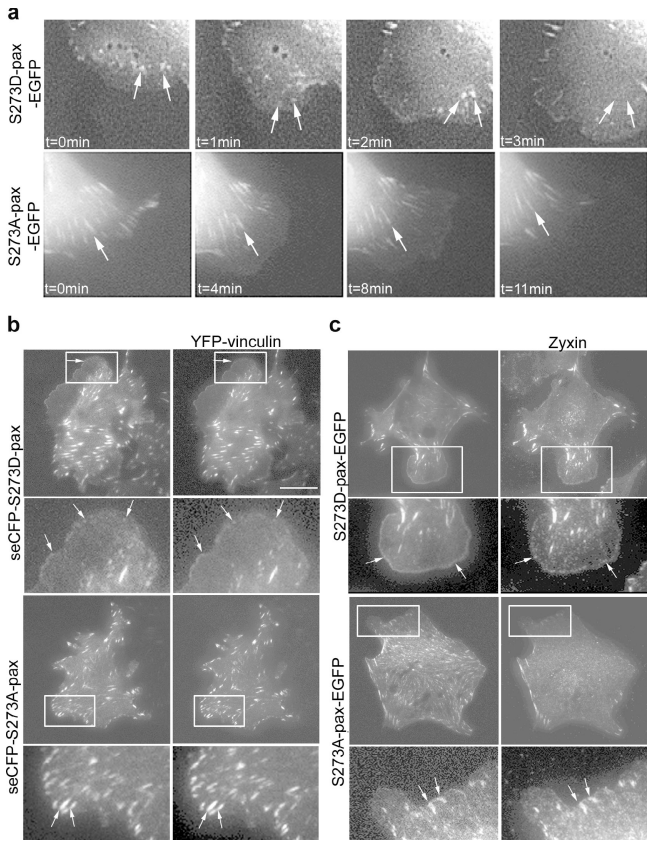


Figure 3. **S273-paxillin phosphorylation induces the formation of small, dynamic adhesions in protrusions.** (a, top) Time-lapse imaging of CHO-K1 cells showed S273D-paxillin-GFP localization in small adhesions that appeared and disappeared (turned over) in 1–2 frames (arrows) near the leading edge. (bottom) On the other hand, S273A-paxillin-GFP localized into large adhesions (arrow) near the base of the protrusion that either tend to slide or disassemble slowly (Table I). (b, top) seCFP-S273D-paxillin and YFP-vinculin exhibit colocalization in small adhesions within protrusions (arrows) of CHO-K1 cells, imaged by TIRF. Enlargements of the boxed regions are at the bottom of each panel. Rates of paxillin and vinculin disassembly in these adhesions were accelerated similarly (Table I), indicating that fast turnover is a property of the entire adhesion. (bottom) In contrast, CHO-K1 cells coexpressing seCFP-S273A-paxillin and YFP-vinculin exhibited larger adhesions (arrows) with similar but slower adhesion disassembly rates (Table I). Bar, 20 μm. (c) S273A- and S273D-paxillin-GFP colocalized with zyxin in small adhesions in protrusive parts of CHO-K1 cells and in larger adhesions at the protrusion base, respectively, as shown in TIRF experiments. Arrows point to the regions where paxillin and zyxin colocalize.

WT-paxillin, S273A-paxillin–expressing CHO-K1 cells displayed shorter migration paths. In contrast, the migration paths of cells expressing S273D-paxillin were significantly longer. We also assayed the protrusiveness of S273D-paxillin–expressing cells that formed many protrusions (unpublished data), unlike S273A-paxillin–expressing cells. Protrusion rates, as assayed by kymography (Fig. 2 b; Hinz et al., 1999), increased sevenfold (10.6 ± 1.3 μm/min) and reduced threefold (0.5 ± 0.1 μm/min) with S273D- and S273A-paxillin, respectively, when compared with WT-paxillin (1.5 ± 0.2 μm/min; Fig. 2 c). The protrusion stability increased twofold (42.0 ± 5.0 min) and decreased slightly for S273A- and S273D-paxillin (17.0 ± 2.0 min), respectively, compared with WT-paxillin (22.0 ± 3.0 min; Fig. 2 d). Therefore, S273-paxillin phosphorylation regulates the migration and protrusive activity of CHO-K1 cells.

Table I. **Apparent $t_{1/2}$ for formation and $t_{1/2}$ for disassembly of paxillin and vinculin in CHO-K1 cells expressing S273-paxillin mutants**

| Expressed protein | Apparent $t_{1/2}$ (adhesion formation) | $t_{1/2}$ (adhesion disassembly) | $t_{1/2}$ (YFP-vinculin disassembly) |
|---|---|---|---|
| | *min* | *min* | *min* |
| WT-pax | 9.5 ± 0.5 | 6 ± 2.5 | 7.0 ± 1.0 |
| S273A-pax | 14 ± 1 | 13 ± 1.5 | 13.7 ± 2.3 |
| S273D-pax | <1 | <1 | <1 |

$t_{1/2}$ is reported as means ± SEM. For each $t_{1/2}$ determination, measurements were obtained for 15–20 individual adhesions on four to six cells from three independent experiments.

## S273-paxillin phosphorylation regulates adhesion dynamics

The LD4 domain of paxillin is implicated in the regulation of adhesion turnover (Webb et al., 2004). Thus, we assayed the effects of S273-paxillin phosphorylation on adhesion turnover by measuring the $t_{1/2}$ for adhesion formation and disassembly in protrusive regions (Webb et al., 2004) of CHO-K1 cells expressing the S273-paxillin mutants. S273D-paxillin expression produced a large number of very small adhesions in the protrusions near the leading edge (Fig. 3 a and Video 1, available at http://www.jcb.org/cgi/content/full/jcb.200509075/DC1). These adhesions formed and disassembled with a $t_{1/2}$ of <1 min (Table I). In contrast, we did not observe these small, dynamic adhesions in the S273A-paxillin–expressing cells; instead, the majority of the adhesions were large and relatively stable (Fig. 3 a, Table I, and Video 2). Cells expressing WT-paxillin showed an intermediate ratio of small to large adhesions (unpublished data). A similar effect on adhesion formation and disassembly was observed in paxillin-null ($pxl^{-/-}$) mouse embryonic fibroblasts (MEFs) expressing S273D- and S273A-paxillin (unpublished data). To determine whether the rapid dynamics was a property of paxillin or of the adhesion as a whole, we imaged CHO-K1 cells coexpressing super-enhanced cyan fluorescent protein (seCFP)–S273D-paxillin and YFP-vinculin using time-lapse total internal reflection fluorescence (TIRF) microscopy (Fig. 3 b). In these cells, the $t_{1/2}$ for paxillin and vinculin disassembly decreased similarly (Table I). On the other hand, CHO-K1 cells coexpressing seCFP-S273A-paxillin and YFP-vinculin exhibited a similar $t_{1/2}$ for adhesion disassembly (Fig. 3 b and Table I). Another adhesion marker, zyxin, colocalized with paxillin in the small adhesions in the protrusive areas of CHO-K1 cells (Fig. 3 c). Thus, S273-paxillin phosphorylation increases adhesion turnover in the protrusive regions of the cell.

## S273-paxillin phosphorylation targets GIT1 near the leading edge

GIT1 is targeted to the leading edge through its interaction with paxillin (Manabe et al., 2002). To corroborate this, we determined endogenous GIT1 distribution in $pxl^{-/-}$ MEFs using TIRF. GIT1 did not localize prominently to adhesions in $pxl^{-/-}$ MEFs, which exhibit large vinculin-containing adhesions (Fig. S2, available at http://www.jcb.org/cgi/content/full/jcb.200509075/DC1). In contrast, both GIT1 and

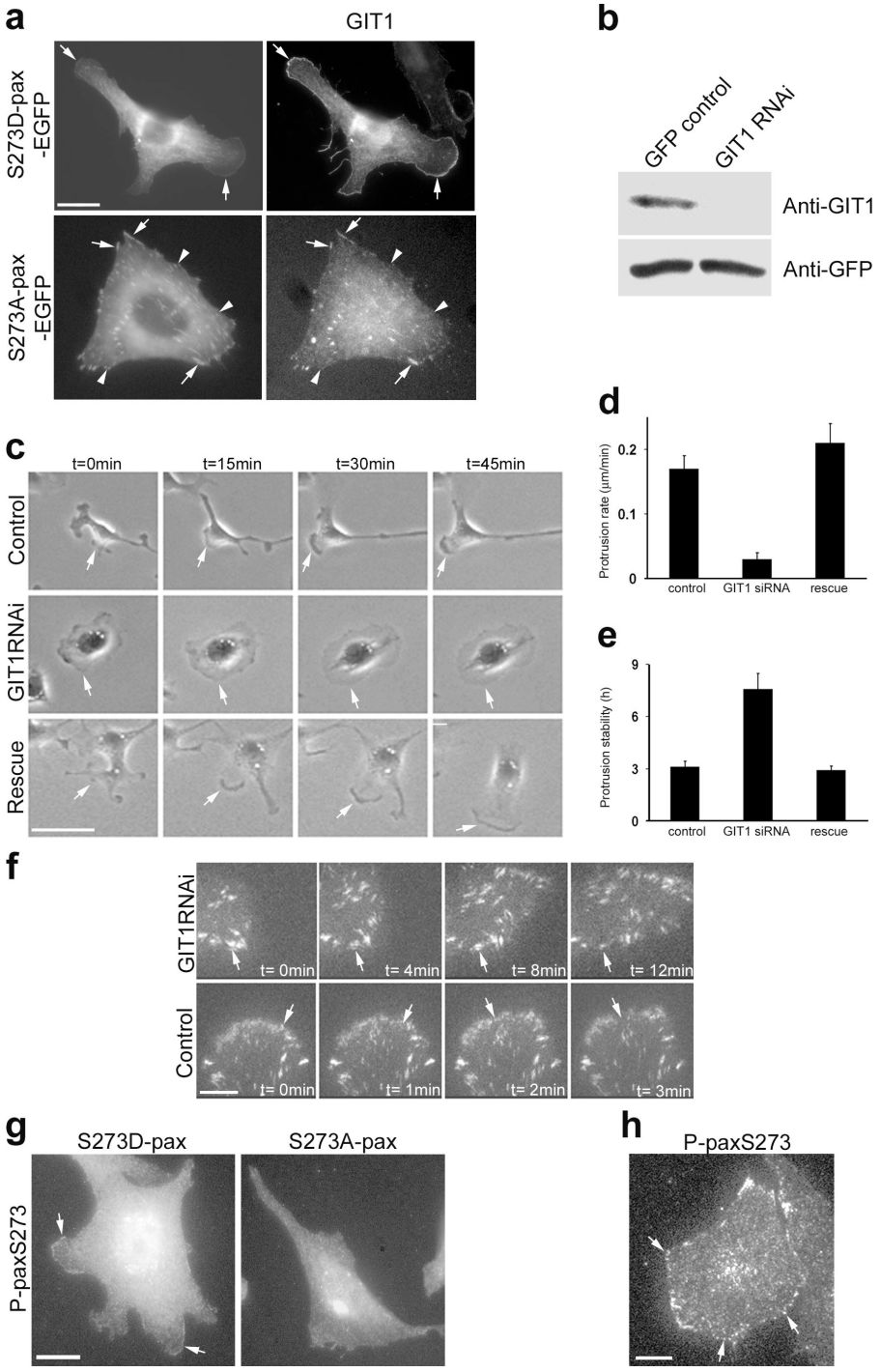


Figure 4. **GIT1 is targeted near the leading edge on S273-paxillin phosphorylation, where it enhances protrusion and adhesion dynamics.** (a, left) Subcellular localization of the paxillin-GFP mutants is shown. (right) GIT1 immunostaining showed that both paxillin and GIT1 localized prominently near the leading edge (arrows) in CHO-K1 cells expressing S273D-paxillin-GFP. However, in S273A-paxillin-GFP–expressing CHO-K1 cells, GIT1 localized weakly in only some of the large adhesions (arrows) but not in others (arrowheads). Bar, 10 μm. (b) Immunoblot of Rat2 lysates coexpressing GFP and either pSUPER vector (control) or GIT1 RNAi. The blot was probed with a GIT1 antibody. GIT1 RNAi, but not pSUPER alone, caused a large decrease in endogenous GIT1 expression. (c) GIT1 knockdown decreases protrusiveness compared with the pSUPER control (arrows show stable and dynamic protrusions, respectively). Coexpression of human GIT1 with rat GIT1 RNAi (rescue) restored the protrusiveness (arrow). Bar, 30 μm. (d) Quantification of protrusion rate. GIT1 RNAi decreased the protrusion rate compared with the control, and this defect was rescued by coexpressing GFP-tagged human GIT1 with rat GIT1 RNAi (rescue). (e) GIT1 knockdown increased protrusion stability compared with control cells, whereas coexpression of GFP-tagged human GIT1 (rescue) decreased it back to control levels. A minimum of eight cells per treatment and at least three protrusions per cell from three independent experiments were analyzed. Error bars represent SEM from three experiments. (f) GIT1 knockdown reduces adhesion turnover. Note that the large adhesions near the cell periphery (arrows) in Rat2 cells coexpressing GIT1 RNAi are more stable than WT-paxillin-GFP–expressing cells. Control cells expressing WT-paxillin-GFP and the pSUPER vector alone show smaller and more dynamic adhesions near the cell periphery (arrows). Bar, 5 μm. (g) Phospho–S273-paxillin immunostaining showed robust localization of phospho–S273-paxillin near the leading edge in S273D-paxillin-GFP–expressing cells but was not readily detected in S273A-paxillin-GFP–expressing cells. Bar, 10 μm. (h) CHO-K1 cells were immunostained for endogenous phospho–S273-paxillin and visualized using TIRF. Endogenous phospho–S273-paxillin localized in small puncta near the leading edge. Bar, 10 μm.

vinculin localized in small adhesions near the cell periphery in WT MEFs (Fig. S2). Because paxillin–GIT1 binding increases upon S273-paxillin phosphorylation, we next asked whether the S273-paxillin mutants affected endogenous GIT1 localization. Both paxillin and GIT1 localized prominently near the leading edge in S273D-paxillin–expressing cells. However, in S273A-paxillin–expressing cells, which have only a few protrusions, GIT1 localized weakly in some large adhesions (Fig. 4 a). We saw a similar effect in CHO-K1 cells coexpressing YFP-GIT1 and seCFP-S273D-paxillin or -S273A-paxillin (unpublished data).

To confirm the role of GIT1 in protrusion dynamics and adhesion turnover, we knocked down GIT1 expression in Rat2 fibroblasts using a GIT1 RNAi. Expression of a rat GIT1 RNAi dramatically reduced GIT1 expression compared with the control pSUPER vector alone (Fig. 4 b). GIT1 RNAi–expressing cells showed a fivefold decrease in the protrusion rate ($0.03 \pm 0.01$ μm/min; Fig. 4, c and d) and a 2.5-fold increase in protrusion stability (Fig. 4 e; $P < 0.0001$) compared with the control ($0.17 \pm 0.02$ μm/min; $P < 0.0001$). To determine whether this is due to loss of GIT1 expression, we rescued the rat GIT1 RNAi–expressing cells by coexpressing human GIT1, which is

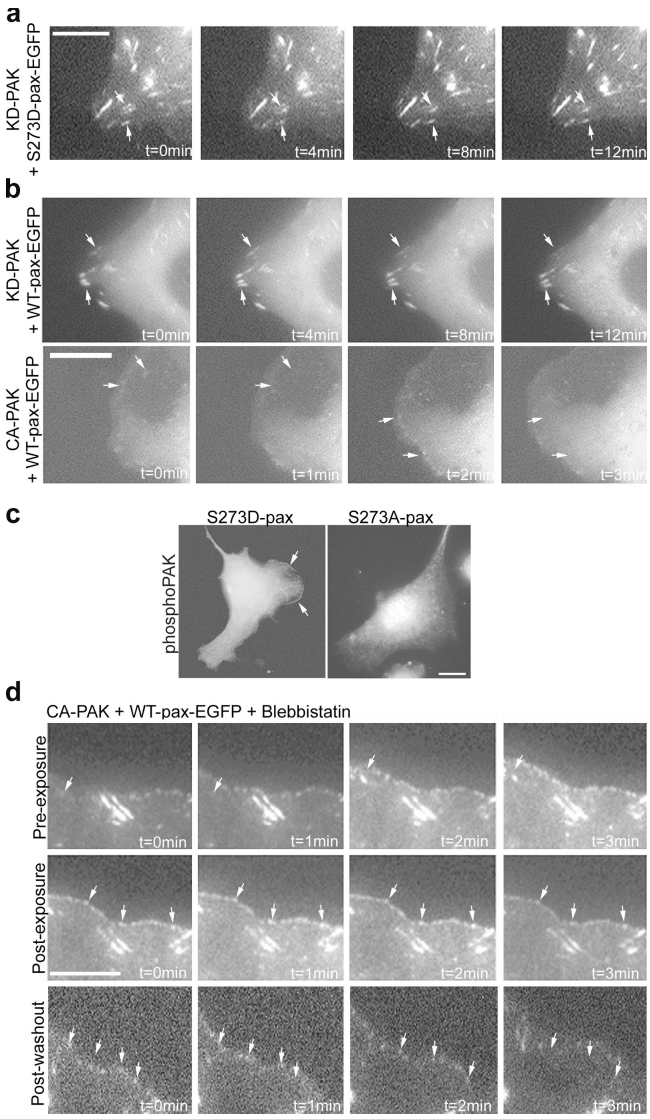


Figure 5. **PAK activation and localization to the leading edge is required for fast adhesion dynamics.** (a) KD-PAK strongly inhibited the S273D-paxillin phenotype. CHO-K1 cells coexpressing KD-PAK and S273D-paxillin-GFP formed large adhesions (arrows) with a reduced disassembly rate. Bar, 5 μm. (b) PAK activation enhances adhesion turnover. (top) CHO-K1 cells coexpressing KD-PAK and WT-paxillin-GFP show large and stable adhesions (arrows) that disassemble slowly (Table II). (bottom) In contrast, note the numerous small and dynamic adhesions (arrows) near the leading edge in cells coexpressing CA-PAK and WT-paxillin-GFP. These adhesions formed and disassembled very rapidly (Table II). Bar, 5 μm. (c) Phospho-PAK immunostaining in CHO-K1 cells expressing S273D- or S273A-paxillin-GFP. The S273D mutant showed robust phospho-PAK localization near the leading edge (arrows), whereas the labeling pattern was diffuse in cells expressing S273A-paxillin. Bar, 20 μm. (d) CHO-K1 cells coexpressing CA-PAK and WT-paxillin-GFP were treated with blebbistatin, a myosin ATPase inhibitor. (top) Small adhesions (arrows) turn over rapidly in the protrusive regions of the cell before exposure to blebbistatin. (middle) Immediately after exposure, protrusion ceased and the adhesions stopped turning over (arrows). (bottom) After washout of blebbistatin, faster adhesion turnover recovered (arrows). Bar, 5 μm.

insensitive to the rat RNAi. This restored both the protrusion rate (0.21 ± 0.03μm/min; Fig. 4, c and d) and stability (Fig. 4 e) to control levels. Also, in cells coexpressing GIT1 RNAi and WT-paxillin, the fraction of adhesions that turned over decreased approximately fourfold compared with control cells. Those that did had an increased $t_{1/2}$ for both adhesion formation ($t_{1/2}$ = 3.5 ± 1.5 min) and disassembly ($t_{1/2}$ = 4.5 ± 1.5 min) compared with control cells coexpressing the pSUPER vector and WT-paxillin ($t_{1/2}$ <1 min; Fig. 4 f). Thus, GIT1 directly regulates both protrusive activity and adhesion turnover.

Table II. **Effect of PAK activation on WT-paxillin dynamics in CHO-K1 cells**

| Expressed protein | Apparent $t_{1/2}$ (adhesion formation) | $t_{1/2}$ (adhesion disassembly) |
|---|---|---|
| | *min* | *min* |
| WT-pax | 9.5 ± 0.5 | 6 ± 2.5 |
| KD-PAK + WT-pax | 18.0 ± 1.5 | 18.8 ± 1.6 |
| CA-PAK + WT-pax | <1 | <1 |

$t_{1/2}$ is reported as means ± SEM. For each $t_{1/2}$ determination, measurements were obtained for 15–20 individual adhesions on four to six cells from three independent experiments.

GIT1 targeting to the leading edge by S273D-paxillin prompted us to examine the subcellular localization of phospho–S273-paxillin, using the phospho–S273-paxillin–specific antibody. S273D-paxillin–expressing CHO-K1 cells revealed robust leading edge localization of phospho–S273-paxillin, whereas it was not readily detected in S273A-paxillin–expressing cells (Fig. 4 g). In CHO-K1 cells, endogenous phospho–S273-paxillin also localized in small puncta near the leading edge (Fig. 4 h) that were not seen upon antibody preincubation with a competitive phosphopeptide (Fig. S3, available at http://www.jcb.org/cgi/content/full/jcb.200509075/DC1). Thus, S273-paxillin phosphorylation promotes both paxillin and GIT1 localization to the leading edge.

## S273-paxillin phosphorylation regulates adhesion dynamics through PAK and myosin

To test whether PAK also functions downstream of S273-paxillin phosphorylation, we cotransfected KD-PAK and S273D-paxillin in CHO-K1 cells. KD-PAK strongly inhibited the S273D-paxillin phenotype (i.e., it reduced protrusive activity) and induced the formation of large adhesions, only a few of which disassembled over time (Fig. 5 a). These adhesions showed an increased $t_{1/2}$ of adhesion disassembly, comparable to that of the S273A-paxillin mutant (Table I). CHO-K1 cells coexpressing KD-PAK and WT-paxillin also displayed reduced protrusiveness (Video 3, available at http://www.jcb.org/cgi/content/full/jcb.200509075/DC1) and the formation of large and stable adhesions (Fig. 5 b), only a few of which disassembled (8 ± 5%). The $t_{1/2}$ for adhesion formation and disassembly for the adhesions that did turn over increased two- and threefold, respectively, compared with cells expressing WT-paxillin alone (Table II). In contrast, CHO-K1 cells coexpressing CA-PAK and WT-paxillin were more protrusive (Video 4) and showed paxillin localization to numerous small and dynamic adhesions (Fig. 5 b) near the leading edge. Most of these adhesions (80 ± 5%) turned over and exhibited a $t_{1/2}$ of <1 min for both adhesion formation and disassembly (Table II). Thus, CA-PAK mimicked the S273D-paxillin phenotype.

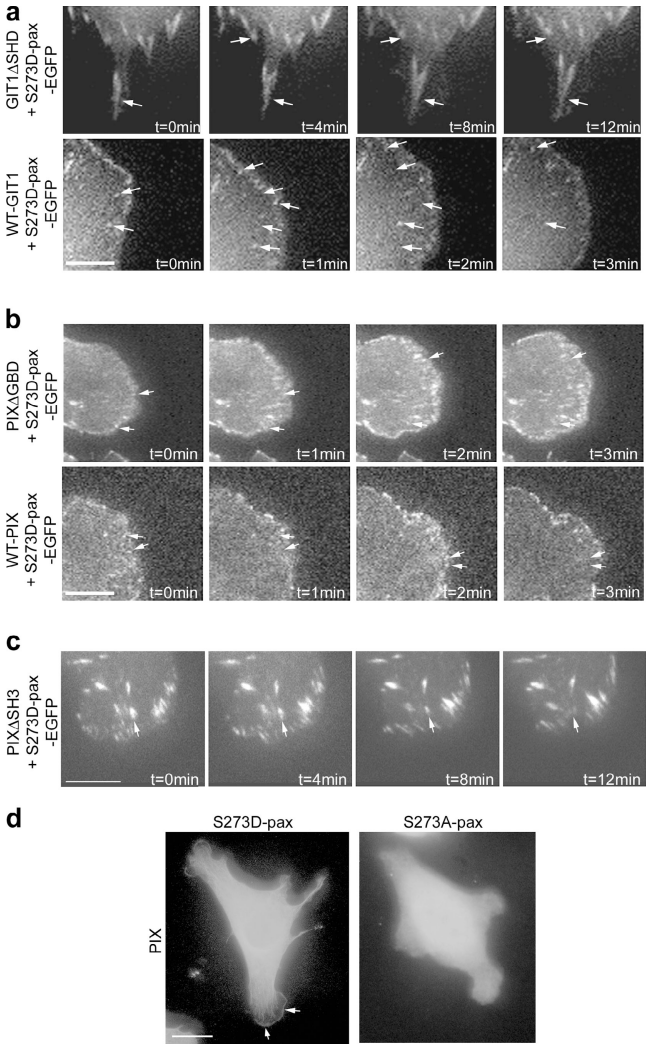


Figure 6. **PIX–GIT1 and PIX–PAK interactions are required for increased protrusion and adhesion dynamics.** (a, top) GIT1ΔSHD coexpression with S273D-paxillin led to the formation of large stable adhesions (arrows; Table III). (bottom) Control CHO-K1 cells coexpressing WT-GIT1 and S273D-paxillin showed small, dynamic adhesions in the protrusive regions of the cell (arrows; Table III). Bar, 5 μm. (b) CHO-K1 cells coexpressing PIXΔGBD and S273D-paxillin show small adhesions that exhibit rapid disassembly (arrows; Table III) in the protrusive regions of these cells. (bottom) Control CHO-K1 cells coexpressing WT-PIX and S273D-paxillin showed small adhesions (arrows) that disassemble very rapidly (Table III) in the protrusive regions of the cell. Bar, 10 μm. (c) Coexpression of PIXΔSH3 with S273D-paxillin in CHO-K1 cells led to the formation of large stable adhesions (arrows; Table III). Bar, 5 μm. (d) Immunostaining for PIX in CHO-K1 cells expressing S273D- or S273A-paxillin-GFP showed robust PIX localization to a region near the leading edge (arrows) in cells expressing S273D-paxillin. In contrast, the leading edge PIX localization was not observed in S273A-paxillin–expressing cells. Bar, 20 μm.

To show that activated PAK resides in the vicinity of dynamic adhesions, we determined its localization using a phospospecific antibody that recognizes T423-phosphorylated active PAK (Sells et al., 2000). Cells expressing S273D-paxillin showed robust phospho-PAK localization near the leading edge, whereas it did not show leading edge localization in cells expressing S273A-paxillin (Fig. 5 c). Thus, S273-paxillin phosphorylation promotes phospho-PAK localization near the leading edge.

Table III. **Effect of GIT1 and PIX mutants on S273D-paxillin disassembly**

| Expressed protein | $t_{1/2}$ (adhesion disassembly) |
|---|---|
| | *min* |
| S273D-pax | <1 |
| GIT1-ΔSHD + S273D-pax | 13.0 ± 0.8 |
| WT-GIT1+ S273D-pax | <1 |
| PIX-ΔGBD + S273D-pax | <1 |
| WT-PIX + S273D-pax | <1 |
| PIX-ΔSH3 + S273D-pax | 16.0 ± 1.1 |
| PIX-LL + S273D-pax | 14.4 ± 2.4 |

$t_{1/2}$ is reported as means ± SEM. For each $t_{1/2}$ determination, measurements were obtained for 15–20 individual adhesions on four to six cells from three independent experiments.

We next asked what regulated adhesion turnover downstream of PAK. Myosin II is regulated by PAK, either through direct phosphorylation of myosin light chain (MLC; Chew et al., 1998) or indirectly, though phosphorylation of MLC kinase (Sanders et al., 1999). To determine whether the turnover of the small paxillin-containing adhesions is dependent on myosin, we treated CHO-K1 cells coexpressing CA-PAK and WT-paxillin with 50 μM blebbistatin, a specific inhibitor of myosin II ATPase activity (Kovacs et al., 2004). Immediately after exposure, the cells stopped protruding and the small adhesions stabilized and did not turn over; upon washout, the fast turnover rate recovered (Fig. 5 d), pointing to myosin as a key effector of this pathway.

### S273-paxillin phosphorylation pathway requires GIT1–PIX and PIX–PAK interaction

Our working hypothesis is that PAK is linked to paxillin indirectly via PIX, which in turn binds to GIT1 (Manabe et al., 2002). To test this hypothesis, we cotransfected CHO-K1 cells with S273D-paxillin and various mutants that disrupt the ternary GIT1–PIX–PAK module, namely, GIT1ΔSHD, PIXΔGBD, or PIXΔSH3. Expression of a GIT1 mutant with a deletion in the PIX binding domain (GITΔSHD) led to S273D-paxillin localization in large and stable adhesions, only a few of which disassembled (Fig. 6 a), with a 13-fold increased $t_{1/2}$ of adhesion disassembly compared with WT-GIT1 control (Table III). However, cells coexpressing a GIT1 binding–deficient PIX mutant (PIXΔGBD) and S273D-paxillin still formed small and dynamic adhesions (Video 5, available at http://www.jcb.org/cgi/content/full/jcb.200509075/DC1), which are indistinguishable from WT-PIX control (Table III and Fig. 6 b) and likely the result of PIX mislocalization, as reported by others (Zhang et al., 2003). In contrast, PIXΔSH3, a PAK binding–deficient PIX mutant (Koh et al., 2001), abrogated the S273D phenotype, i.e., it led to decreased protrusiveness (Video 6) and formation of large and stable adhesions (Fig. 6 c). Of those, only a few disassembled with a 16-fold increased $t_{1/2}$ for adhesion disassembly compared with WT-PIX control (Table III and Fig. 6 a). These results strongly implicate a requirement for GIT1–PIX–PAK interaction for fast adhesion dynamics.

We examined PIX localization in CHO-K1 cells expressing the S273-paxillin mutants. PIX localized robustly to a region near the leading edge in CHO-K1 cells expressing

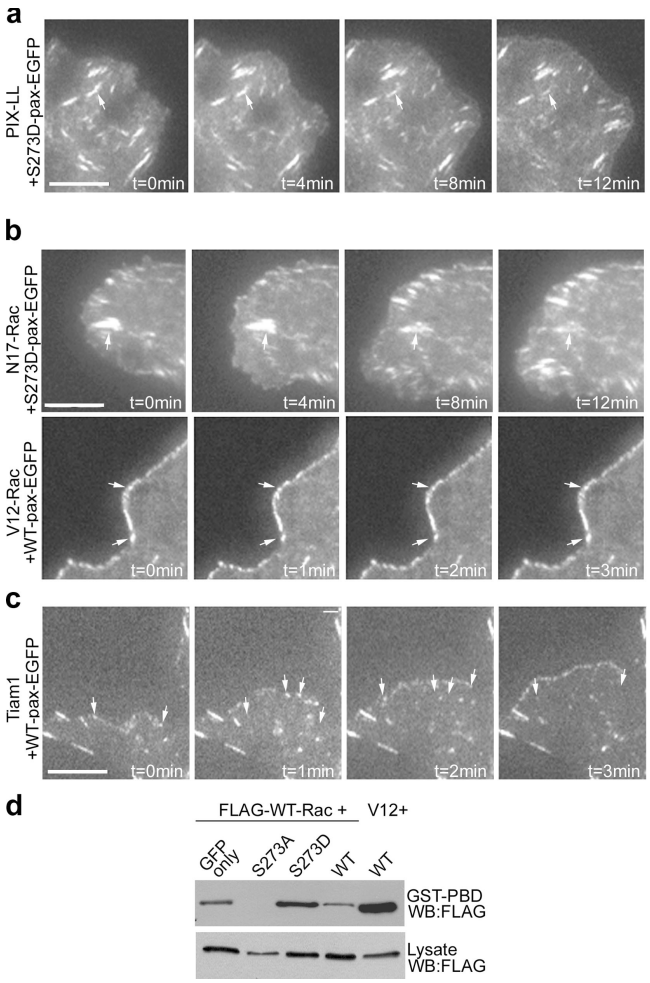


Figure 7. **Rac activation regulates adhesion turnover.** (a) CHO-K1 cells coexpressing S273D-paxillin-GFP and a PIX mutant, which lacks nucleotide exchange activity (PIX-LL) showed large adhesions (arrows) that disassembled slowly (Table III). Bar, 5 μm. (b, top) CHO-K1 cells coexpressing dominant-negative (N17-Rac) and S273D-paxillin-GFP show large and stable adhesions (arrows) that disassemble slowly (Table IV). (bottom) CHO-K1 cells coexpressing CA- (V12-Rac) and WT-paxillin-GFP exhibit numerous small but stable adhesions (Table IV) at the cell periphery (arrows). Bar, 5 μm. (c) CHO-K1 cells coexpressing the Rac GEF Tiam1 and WT-paxillin-GFP show numerous small paxillin-containing adhesions (arrows) that disassemble very rapidly (Table IV). Bar, 5 μm. (d) S273-paxillin phosphorylation increases Rac activation. Rac activity from CHO-K1 lysates coexpressing FLAG-WT-Rac and paxillin-GFP mutants was measured using a GST-PBD pull-down assay. CHO-K1 lysates coexpressing FLAG-V12-Rac and WT-paxillin-GFP served as a positive control. (top) Active Rac in GST-PBD bead pellets was detected by immunoblotting using an anti-FLAG antibody. (bottom) Equal protein aliquots of lysates served as loading controls. Rac activation increased eightfold with S273D-paxillin when compared with S273A-paxillin and 1.5-fold compared with WT-paxillin.

S273D-paxillin. In contrast, PIX leading edge localization was not observed in S273A-paxillin–expressing cells (Fig. 6 d). These data indicate that PIX localizes to a region near the leading edge in response to S273-paxillin phosphorylation.

### The PIX–PAK interaction functions through Rac

PIX exhibits exchange factor activity for small GTPases, including Rac, which in turn can promote protrusive activity and adhesion formation (Ridley, 2001). To determine whether this activity is required for the effects of PIX, we used a guanine nucleotide exchange factor (GEF)–deficient mutant, PIX-LL (L238R and L239S; Manser et al., 1998). Coexpression of the PIX-LL mutant with S273D-paxillin in CHO-K1 cells induced the formation of large adhesions (Fig. 7 a) that showed a 14-fold increase in the $t_{1/2}$ for adhesion disassembly when compared with S273D-paxillin alone (Table III). The role of Rac was further confirmed by cotransfecting CHO-K1 cells with dominant-negative N17-Rac and S273D-paxillin. In addition to reducing protrusiveness (Video 7, available at http://www.jcb.org/cgi/content/full/jcb.200509075/DC1), N17-Rac expression gave rise to large and stable adhesions with a 16-fold increased $t_{1/2}$ for adhesion disassembly (Table IV and Fig. 7 b). On the other hand, CHO-K1 cells coexpressing V12-Rac and WT-paxillin exhibited numerous small adhesions around the cell periphery (Fig. 7 b and Video 8). However, the cells were not protrusive and the adhesions were not dynamic (Fig. 7 b, Table IV, and Video 8). We then transfected CHO-K1 cells with WT-paxillin and Tiam1, a potent Rac GEF. Tiam1 expression, like PIX, led to the formation of small adhesions (Fig. 7 c) that turned over rapidly (Table IV). These data suggest a requirement of Rac GTPase cycling for fast adhesion dynamics.

Table IV. **Effect of Rac activation on S273D- and WT-paxillin dynamics**

| Expressed protein | $t_{1/2}$ (adhesion disassembly) |
|---|---|
| | *min* |
| S273D-pax | <1 |
| N17Rac + S273D-pax | 15.9 ± 0.8 |
| V12Rac + WT-pax | nd |
| Tiam1 + S273D-pax | <1 |

$t_{1/2}$ is reported as means ± SEM. For each $t_{1/2}$ determination, measurements were obtained for 15–20 individual adhesions on four to six cells from three independent experiments. nd represents stable adhesions that did not turn over at all.

We next assayed for active Rac in cells expressing the S273-paxillin phosphomutants using a GST–p21 binding domain (PBD) pull-down assay. CHO-K1 cells coexpressing FLAG-WT-Rac and WT-, S273A-, S273D-paxillin-GFP or GFP vector alone were lysed 24 h after transfection, and Rac activity was assayed by its binding to the GST fusion of the PBD (Fig. 7 d). The positive control with WT-paxillin-GFP and V12-Rac exhibited maximum Rac-GTP binding to the GST-PBD bait. S273A-paxillin-GFP expression induced a marked decrease of bound Rac (approximately fourfold; $n = 3$), whereas the GFP control and WT-paxillin-GFP showed comparable levels of bound Rac. Rac activation increased eightfold with S273D-paxillin when compared with S273A-paxillin and 1.5-fold when compared with WT-paxillin. Thus, S273-paxillin phosphorylation induces Rac activation.

### The nature of the small, dynamic adhesions

Using TIRF, we observed numerous small, highly dynamic adhesions near the leading edge of S273D-paxillin–expressing CHO-K1 cells (Fig. 8 a and Video 9, available at http://www.jcb.org/cgi/content/full/jcb.200509075/DC1) and in other cell types, including NIH 3T3 fibroblasts and WT MEFs expressing S273D-paxillin (not depicted). Using high time resolution TIRF

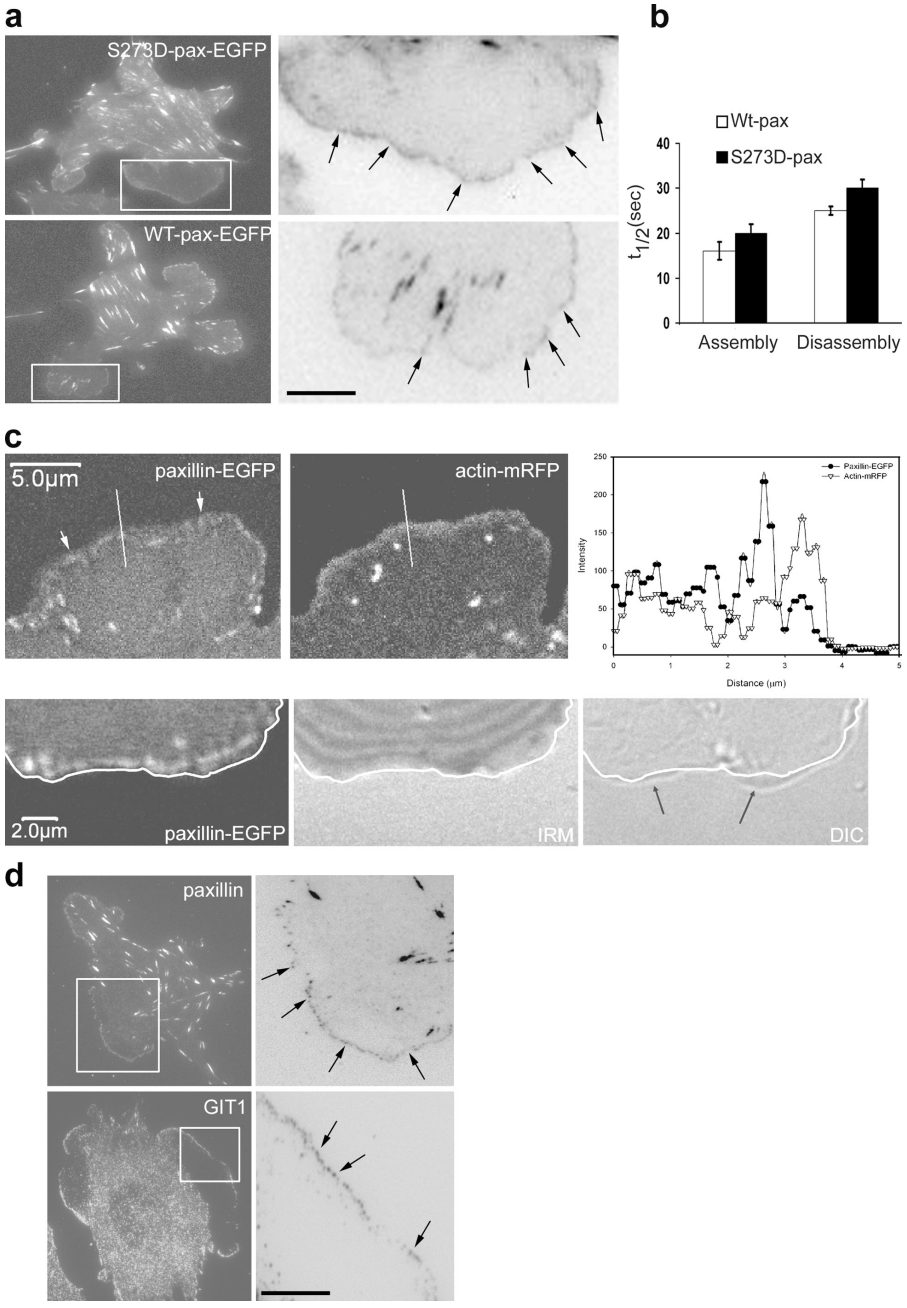


Figure 8. **Characterization of the small and dynamic adhesions near the leading edge.** (a) TIRF visualization of S273D- and WT-paxillin adhesions. Numerous small adhesions are seen along the leading edge in the S273D- as well as WT-paxillin–expressing cells. Enlargements of the boxed regions are shown in the right panels as inverse images (arrows show small adhesions near the leading edges). Bar, 5 μm. (b) Adhesion turnover assay using high time resolution imaging (time intervals ~3–5 s). Both S273D- and WT-paxillin containing small adhesions turned over at similar rates. The error bars represent SEM from independent experiments. For each condition, 40–60 adhesions from 8–10 different cells were analyzed. (c, top) CHO-K1 cells coexpressing WT-paxillin-GFP and actin–monomeric RFP showed small adhesions (arrows) near the leading edge ~1 μm behind the peak intensity of the actin band (compare black circles to open triangles). Bar, 5 μm. (bottom) Coincidence between paxillin, IRM, and DIC images. The leading edge is ahead of the paxillin-containing adhesions and does not overlap with the IRM signal, showing that it is not attached to the substratum. Bar, 2 μm. (d) TIRF visualization of endogenous paxillin and GIT1 in CHO-K1 cells. Both localized in the small adhesions near the leading edge (arrows). Enlargements of the boxed regions are shown in the right panels as inverse images. Bar, 5 μm.

imaging, we measured a $t_{1/2}$ of 30 ± 2 s for adhesion disassembly and 20 ± 1 s for assembly for S273D-paxillin (Fig. 8 b). To find out whether these adhesions were present under normal conditions, we examined cells expressing WT-paxillin using TIRF. An array of small and transient adhesions that are not readily apparent using wide-field configurations lined the region near the leading edge in the protrusive regions (Fig. 8 a and Video 10). These adhesions showed a $t_{1/2}$ of 16 ± 2 s and 25 ± 2 s for adhesion formation and disassembly, respectively, suggesting that these adhesions are similar to those seen in S273D-paxillin–expressing cells (Fig. 8 b). Quantitative measurements of the adhesion size from their intensity profiles gave a diameter of 0.5 ± 0.1 μm, which did not vary with intensity, suggesting that they are subresolution.

To determine the location of these adhesions with respect to the leading edge, we superimposed differential interference contrast (DIC) and fluorescence images of CHO-K1 cells expressing WT-paxillin. These adhesions were located 0.5–1.0 μm behind the leading edge (Fig. 8 c). Furthermore, cells coexpressing WT-paxillin-GFP and actin–monomeric RFP showed actin localization in a fluorescent band at the leading edge, whereas the small paxillin-containing adhesions localized at the boundary between the actin band and the remainder of the lamellipod (Fig. 8 c). In addition, interference reflection microscopy (IRM) showed that these adhesions are in very close proximity to the underlying glass coverslip, whereas the leading edge containing the actin band is above the surface (Fig. 8 c).

Using TIRF, these small adhesions were also seen endogenously in CHO-K1 cells immunostained for paxillin and GIT1 (Fig. 8 d). In addition, these adhesions were observed in highly protrusive tumor-derived cells expressing WT-paxillin-GFP (e.g., B16 melanoma and MDA-MB-231 breast carcinoma cells), whereas a less protrusive MCF7 cell line showed larger and more stable adhesions (unpublished data). Quantification of protrusion rates and adhesion turnover in these cell lines revealed that increased protrusion rates inversely correlated with the $t_{1/2}$ of adhesion formation and disassembly (Table V). The presence of these small paxillin-containing adhesions and their dynamics in these cells suggests that these are a salient feature of highly protrusive cell types.

Table V. **Protrusion rates and adhesion kinetics in tumor-derived cells expressing WT-paxillin-GFP**

| Cell type | Protrusion rate | Apparent $t_{1/2}$ (adhesion formation) | $t_{1/2}$ (adhesion disassembly) |
|---|---|---|---|
| | *μm/min* | *s* | *s* |
| B16 melanoma | 0.76 ± 0.09 | 59 ± 6 | 48 ± 7 |
| MDA-MB-231 | 0.43 ± 0.06 | 129 ± 18 | 56 ± 10 |
| MCF7 | 0.26 ± 0.05 | 207 ± 27 | 105 ± 15 |

Protrusion rates are reported as means ± SEM. For protrusion rate determination, measurements were obtained for 9–15 protrusions from cells from three to five independent experiments. $t_{1/2}$ is reported as means ± SEM. $t_{1/2}$ measurements were obtained for 10 individual adhesions on four to six cells from three independent experiments.

## Discussion

Adhesion turnover at the front of a migrating cell appears to regulate migration by localizing and stabilizing the protrusion as the cell extends forward (adhesion–protrusion coupling). Previous studies implicate FAK, Src, and paxillin in the regulation of adhesion turnover, as *FAK*$^{-/-}$, *SYF*$^{-/-}$, and *pxl*$^{-/-}$ cells exhibit impaired adhesion disassembly, protrusion, and migration (Webb et al., 2004). We describe a novel PAK-mediated phosphorylation pathway that accelerates adhesion turnover and protrusion dynamics in migrating cells. Phosphorylation of paxillin on S273 by PAK promotes the localization of a signaling module containing the adaptor GIT1, the Rac GEF PIX, and the active form of the Rac effector PAK to a region near the leading edge. We conclude that PAK acts both upstream and downstream of S273-paxillin phosphorylation, in a positive-feedback loop, providing a mechanism for adhesion–protrusion coupling.

It is tempting to speculate that the pax–GIT1–PIX–PAK module localizes Rac activity near the leading edge through the joint presence of PIX and PAK. This is consistent with previous studies that show Rac localization near the leading edge (Kraynov et al., 2000) and our own observation that Rac activation and cycling is required for rapid adhesion turnover. Genetic studies in *Drosophila melanogaster* also implicate a positive role for paxillin in the regulation of Rac activity (Chen et al., 2005). Finally, recent evidence shows that the Rac-dependent spatial localization of protrusive activity is mediated by active PAK through the recruitment of PIX (Cau and Hall, 2005; Zhang et al., 2005).

Our results demonstrate that active PAK is a key effector for fast adhesion turnover and protrusion dynamics after S273-paxillin phosphorylation. These observations are consistent with previous studies that have hinted at a role for PAK in adhesion stability (Manser et al., 1997) and shown active PAK localization near the leading edge (Sells et al., 2000). We have extended these observations by clarifying the function and location of active PAK, demonstrating its direct role in adhesion turnover, and providing a pathway for regulating its localization.

How does PAK regulate the rapid turnover of the highly dynamic adhesions? The inhibition of adhesion turnover by blebbistatin suggests that myosin is a major effector. PAK is known to affect myosin activity both by inhibiting MLC kinase (Sanders et al., 1999) and through the direct phosphorylation of MLC (Chew et al., 1998). Although the ATPase activity of myosin II generates contractile forces that are thought to mediate adhesion assembly (Chrzanowska-Wodnicka and Burridge, 1996), there is also evidence that such contractility is involved in adhesion disassembly (Crowley and Horwitz, 1995). Thus, there are several possibilities for myosin-mediated regulation of adhesion turnover.

The effect of PAK on protrusion also has multiple possibilities. A likely candidate is its effector LIM kinase, which regulates actin dynamics by inactivating actin depolymerizing factor/cofilin family members (Edwards et al., 1999). Modulating adhesion to the substratum is another possibility, as net protrusion is thought to result from the balance between actin treadmilling, retrograde actin flow, and the interaction of the actin filaments with adhesions (Mitchison and Kirschner, 1988). Increased interaction with adhesions leads to more traction, less retrograde flow, and, hence, higher protrusion rates (Lin and Forscher, 1995).

Although our results show a positive regulatory role for GIT1 at the leading edge, a recent study (Nishiya et al., 2005) in $\alpha_4$ integrin–expressing cells demonstrates an ARF–GTPase-activating protein domain–mediated inhibitory role for GIT1 at the sides and rear of migrating cells. This suggests that GIT1 serves complementary roles depending on the spatial cellular context. Though the events controlling adhesion signaling and migration via the $\alpha_4$ or $\alpha_5$ integrins differ substantially (Mostafavi-Pour et al., 2003), our studies do not exclude a role for the ARF–GTPase-activating protein domain of GIT1 in regulating protrusion.

Our results show that S273-paxillin is a highly labile and regulated phosphorylation site. Interestingly, paxillin interacts directly with the serine/threonine phosphatase PP2A (Ito et al., 2000), whose inhibition is observed in certain types of cancer and results in hyperphosphorylation of paxillin serine residues and dissolution of FAK–Src–paxillin complexes (Young et al., 2002; Romashko and Young, 2004). This suggests that S273-paxillin phosphorylation might also be under regulation by phosphatases opening a new facet of adhesion turnover regulation through paxillin dephosphorylation.

Finally, the small adhesions that we observed have interesting properties that distinguish them from other adhesions. They are small (<0.5 μm), turnover rapidly (<1 min), contain GIT1 (as well as other components, such as FAK, vinculin, and zyxin),

and reside in a region ~1 μm behind the leading edge, which also contains phospho-PAK and PIX. They are present in the protrusive regions of normal cells and also highly motile tumor cells. Interestingly, rapidly locomoting cell types such as keratocytes (Lee and Jacobson, 1997), neutrophils (Yuruker and Niggli, 1992), and macrophages (Heiple et al., 1990) do not show highly organized adhesions. In contrast, most other adhesions are large, elongated, and centrally located; turnover with slower rates (several minutes); and do not have prominent concentrations of GIT1. Slower moving cells, e.g., fibroblasts, form these larger adhesions, whose presence corresponds with a decrease in the migration rate (Couchman and Rees, 1979). Therefore, we propose that these small, dynamic adhesions drive the migration of highly motile cells and therefore deserve intense study.

## Materials and methods

**Cell culture and transfection**

CHO-K1 cells were cultured in low-glucose DME supplemented with 10% FBS, 4 mM L-glutamine, 1 mM sodium pyruvate, 1% (vol/vol) nonessential amino acids, and penicillin/streptomycin and transfected with 0.25–1 μg DNA using Lipofectamine (Invitrogen). *Pxl*$^{-/-}$ MEFs and Rat2 fibroblasts were cultured in high-glucose DME supplemented with 10% FBS and penicillin/streptomycin. Rat2 cells were transfected with 0.5–3.0 μg DNA using nucleofection. Cells were incubated 24–72 h before observation.

**Plasmids**

Quickchange mutagenesis kit (Stratagene) was used to introduce the S273 mutations into paxillin-GFP (Laukaitis et al., 2001). 5′-GAGCTGATGGCGGCCCTCTCTGAC-3′ and 5′-GTCAGAGAGGGCCGCCATCAGCTC-3′ primers (forward and reverse) were used to generate S273A-paxillin. For S273D-paxillin, the primers used were 5′-GAGCTGATGGCGGACCTCTCTGAC-3′ and 5′-GTCAGAGAGGTCCGCCATCAGCTC-3′. Both mutations were confirmed using the sequencing primer 5′-CGTGTCAACGCCAGTCAGCAG-3′. seCFP-WT-paxillin was made by subcloning paxillin cDNA from paxillin-pcDNA3.1 Zeo (Laukaitis et al., 2001) into the seCFP vector pKseCFP (a gift from A. Miyawaki, RIKEN, Saitama, Japan) using BamHI and EcoRI restriction sites. S273A and -D mutations were similarly introduced into seCFP-WT-paxillin using the Quickchange mutagenesis kit.

The FLAG-paxillin, untagged WT-paxillin, FLAG-GIT1, GIT1ΔSHD, GIT1RNAi, PIXΔGBD, and PIXΔSH3 constructs were described previously (Manabe et al., 2002; Zhang et al., 2003, 2005; Webb et al., 2005). Myc-FAK (J.T. Parsons, University of Virginia, Charlottesville, VA), CA- and KD-myc-PAK1 (J. Chernoff, Fox Chase Cancer Center, Philadelphia, PA), Rac1 (A. Hall, University College London, London, UK), Tiam1 (J. Collard, The Netherlands Cancer Institute, Amsterdam, Netherlands), HA-βPix (C. Turner, State University of New York Upstate Medical University, Syracuse, NY), HA-PIX-LL (L. Santy and J. Casanova, University of Virginia, Charlottesville, VA), and YFP-vinculin (S. Craig, The Johns Hopkins School of Medicine, Baltimore, MD) constructs were all gifts.

**Antibodies and reagents**

Blebbistatin and CalyculinA were obtained from Calbiochem; DME from GIBCO BRL; fibronectin, protease inhibitor cocktail, Protein A–agarose beads, mouse-IgG beads, and anti-FLAG M2-conjugated agarose from Sigma-Aldrich; glutathione–Sepharose beads and ECL detection system from GE Healthcare, CCM1 from Hyclone, Nucleofection kit from Amaxa Biosytsems, and TnT T7-coupled reticulocyte lysate system from Promega.

The following primary antibodies were used: paxillin (BD Biosciences), c-myc 9E10 (Santa Cruz Biotechnology, Inc.), FLAG M2 (Stratagene), and GFP A-11122 (Invitrogen). The B71 zyxin (M.C. Beckerle, University of Utah, Salt Lake City, UT), phospho-PAK (J. Chernoff), and βPIX antibodies (B. Xiao, The Johns Hopkins University, Baltimore, MD) were gifts. The GIT1 polyclonal antibody was previously described (Manabe et al., 2002).

A polyclonal phospho–S273-paxillin antibody was generated by Biosource International against a chemically synthesized peptide Ac-DELMA[pS]LSDFK-amide that is phosphorylated at S273-paxillin. The antibody was purified from rabbit serum by sequential epitope-specific chromatography, followed by negative preadsorption using a nonphospho–S273-paxillin peptide to remove antibody reactive to nonphosphorylated paxillin. The final product was generated by affinity chromatography using the phospho–S273-paxillin mimetic peptide.

The following secondary antibodies were used: HRP anti–mouse IgG and anti–rabbit IgG (GE Healthcare), Rhodamine anti–mouse and anti–rabbit IgG (MP Biomedicals), Alexa Fluor 555 anti–mouse antibody and anti–rabbit antibody (Invitrogen).

**In vitro transcription–translation coupled kinase assay**

In vitro transcription–translation was performed using the TnT T7-coupled reticulocyte lysate system. 0.5 μg FLAG-paxillin and 0.75 μg of either CA- or KD-myc-PAK1 in T7-containing plasmids were transcribed and translated for 90 min at 30°C. After 90 min, kinase buffer containing 20 mM Hepes, 10 mM NaCl, 1 mM $MgCl_2$, 1 mM $MnCl_2$, and 20 μM ATP was used. The reaction was then allowed to continue for another 30 min at 30°C. For binding experiments, untagged WT-paxillin and FLAG-GIT1 were synthesized using the TnT system and incubated for 30 min with either CA- or KD-myc-PAK1 in kinase buffer. Phosphopeptide competition was performed by preincubating in vitro–synthesized mixtures of untagged WT-paxillin, FLAG-GIT1, and CA-myc-PAK1 with 500 molar excess of the phospho– or nonphospho–S273-paxillin peptide for 30 min. Immunoprecipitation was performed using anti-FLAG M2-conjugated agarose. Proteins were separated by 7.5% SDS-PAGE; transferred to Immobilon membranes; and probed with the phospho–S273-paxillin, anti-FLAG, anti-myc, or anti-paxillin antibodies.

**Immunoprecipitation and Western blotting**

Cells were grown to 80–90% confluency, washed with ice-cold PBS, and lysed with ice-cold lysis buffer (25 mM Tris-HCl, pH 7.4, 100 mM NaCl, 0.5% NP-40, and protease inhibitors). The lysates were incubated on ice for 30 min and clarified by centrifugation (12,000 *g* for 5 min). Equivalent amounts of the lysates were precleared with 30 μl mouse IgG agarose for 1.5 h at 4°C, followed by incubation with 2 μg of the anti-GFP polyclonal antibody for 1.5 h at 4°C. Complexes were incubated with protein A–agarose for 1 h and washed three times with ice-cold lysis buffer. The immunoprecipitates were analyzed by SDS-PAGE on 10% slabs, transferred to nitrocellulose, and detected by Western blot analysis. Protein binding levels were compared by densitometry of scanned Western blots using ImageJ software (NIH). Background-corrected densities were measured and normalized to GFP-paxillin densities run on the same gel.

**Rac activity assay**

The GST-PBD fusion protein was purified with glutathione–Sepharose beads, and assays were performed as described previously (Ren et al., 1999). CHO-K1 cells were cotransfected with FLAG-WT-Rac and GFP vector, WT-paxillin-GFP, S273A- paxillin-GFP, or S273D-paxillin-GFP. A positive control with CHO-K1 cells cotransfected with FLAG-V12-Rac and WT-paxillin-GFP was included. Lysates were collected 24 h after transfection and processed as described elsewhere (Ren et al., 1999).

**Microscopy and image processing**

For live cell imaging, CHO-K1 and Rat2 cells were plated on 1–2 μg/ml fibronectin–coated glass-bottomed dishes in CCM1 for 1 h and maintained at 37°C and pH 7.4. For phase analyses, time-lapse images were captured at 10× (NA 0.50; Nikon) with a charge-coupled device camera (Orca II; Hamamatsu) attached to an inverted microscope (TE-300; Nikon). To quantify adhesion turnover, fluorescence images were captured at 60× (NA 1.40; Nikon). Image acquisition was controlled using ISee (Inovision) or Metamorph (Universal Imaging Corp.) interfaced to a Ludl modular automation controller (Ludl Electronic Products). For EGFP and rhodamine/alexa, an endow GFP filter cube (excitation HQ470/40 and emission HQ525/50; Q495LP dichroic mirror [Chroma Technology]) and a rhodamine/TRITC cube (excitation BP520-550 and barrier filter BA580IF; DM565 dichroic mirror, [Chroma Technology]) were used, respectively. Exposure times ranged from 0.05 to 0.20 s, and time intervals ranged from 3–60 s.

DIC images for kymograph analyses were obtained on an inverted microscope (IX70; Olympus) at 40× (NA 0.60; Olympus). Confocal images were collected on a 300 scanhead (Fluoview 300; Olympus) on the inverted microscope fitted with a 60× PlanApo oil-immersion objective (NA 1.40; Olympus). GFP and RFP were excited using the 488-nm laser line of an Ar ion laser and the 543-nm laser line of a He-Ne laser (Melles Griot), respectively. A Q500LP dichroic mirror (Chroma Technology) was used for GFP-labeled cells. For dual-color GFP-RFP imaging, a green-red cube (488/543/633) with a DM570 dichroic mirror (Chroma Technology) was used. Fluorescence and DIC images were acquired using Fluoview software (Olympus).

For acquiring TIRF images, the IX70 inverted microscope equipped with an objective-based TIRF system (Olympus) was used. The excitation laser lines used were as described for confocal microscopy. A dichroic mirror (HQ485/30) was used for GFP-labeled cells. For dual GFP-RFP and CFP-YFP imaging, a dual emission filter (z488/543) and a dual dichroic mirror (emitter, z457/514; beamsplitter, z457/514) were used, respectively. In addition, clean-up filters were used for GFP (Z488/10), CFP (Z458/10), and YFP (514/10). Chroma Technology supplied all mirrors and filters. Images were acquired with a charge-coupled device camera (Retiga Exi; Qimaging) and analyzed using Metamorph software.

**Immunofluorescence**

Cells were plated on fibronectin-coated glass-bottomed 35-mm dishes (Palecek et al., 1996) in CCM1 medium and fixed with 3% formaldehyde for 15 min. 0.15 M glycine was added for 10 min to stop the fixation followed by permeabilization with 0.2% (vol/vol) Triton X-100 for 5 min at room temperature. For immunostaining phospho–S273-paxillin, PIX, and phosphoactive PAK, the cells were fixed for 3–5 min with 3% formaldehyde, followed by chilled methanol for 15 min. After each step, the cells were washed three times with PBS, blocked with 2% BSA in PBS for 1 h, and incubated with primary antibodies for 1 h, followed by fluorescently conjugated secondary antibodies for 1 h at room temperature. The antibodies were diluted in PBS containing 2% BSA. Slips were mounted on slides with Vectashield mounting media (Vector Laboratories). For TIRF observation, coverslips were mounted using Slowfade antifade kit (Invitrogen).

**Cell migration and protrusion assays**

Cell migration data was generated from time-lapse phase micrographs, and the XY-centroids were determined using Scion Image (NIH). Mean migration rate for each cell was determined by dividing the mean net displacement of the cell centroid divided by the time interval (5 min). Wind Rose plots were generated by transposing individual cell tracks to a common origin.

Protrusion parameters were quantified using kymography (Hinz et al., 1999). For CHO-K1 and Rat2 cells, images were captured at 30-s intervals for 60- and at 5-min intervals for 5 h, respectively. Kymographs were generated using ImageJ or Metamorph software along 1-pixel-wide regions oriented along the protrusion direction and perpendicular to the lamellipodial edge. Straight lines were drawn from the beginning to the end of single protrusion events in the kymographs; retraction events were ignored. Protrusion rates and protrusion stability were calculated from the slopes and x axis projection distance of these lines, respectively. A minimum of eight cells per treatment and at least three protrusions per cell from three independent experiments were analyzed.

**Quantification of adhesion dynamics**

ImageJ or Metamorph software were used to measure the background-corrected fluorescent intensity of individual adhesions over time from cells expressing fluorescently tagged paxillin or vinculin (Webb et al., 2004). Paxillin and vinculin incorporation into and departure from adhesions were linear on semilogarithmic plots of the background-corrected fluorescent intensity as a function of time. The $t_{1/2}$ for formation and disassembly was determined from the slopes of these graphs. For each $t_{1/2}$ determination, measurements were obtained for 15–20 individual adhesions on four to six cells from three independent experiments.

**Online supplemental material**

Fig. S1 shows that phospho–S273-paxillin antibody is specific and phospho–S273-paxillin levels are up-regulated during cell spreading. Fig. S2 shows GIT1 and vinculin distribution in *pxl*$^{-/-}$ and WT MEFs. Fig. S3 shows endogenous phospho–S273-paxillin staining in CHO-K1 cells subject to peptide competition. Videos 1 and 2 show S273D- and S273A-paxillin-GFP dynamics in CHO-K1 cells. Videos 3 and 4 show WT-paxillin-GFP dynamics in CHO-K1 cells coexpressing KD- or CA-PAK and WT-paxillin. Videos 5–7 show S273D-paxillin-GFP dynamics in CHO-K1 cells coexpressing S273D-paxillin and PIXΔGBD, PIXΔSH3, or N17-Rac. Video 8 shows WT-paxillin dynamics in a CHO-K1 cell coexpressing V12-Rac and WT-paxillin. Videos 9 and 10 are TIRF videos of CHO-K1 cells expressing S273D- or WT-paxillin-GFP, respectively. Online supplemental material is available at http://www.jcb.org/cgi/content/full/jcb.200509075/DC1.

We would like to thank Drs. T.J. Parsons, A. Hall, J. Collard, Jonathan Chernoff, Susan Craig, Chris Turner, Bo Xiao, Lorraine Santy, and Jim Casanova for generously providing reagents. We thank Emily L. Whitmore for her help with image analysis.

This work was supported by National Institutes of Health grant GM23244 and the Cell Migration Consortium.

Submitted: 12 September 2005
Accepted: 14 April 2006

## References

Brown, M.C., and C.E. Turner. 2004. Paxillin: adapting to change. *Physiol. Rev.* 84:1315–1339.

Cau, J., and A. Hall. 2005. Cdc42 controls the polarity of the actin and microtubule cytoskeletons through two distinct signal transduction pathways. *J. Cell Sci.* 118:2579–2587.

Chen, G.C., B. Turano, P.J. Ruest, M. Hagel, J. Settleman, and S.M. Thomas. 2005. Regulation of Rho and Rac signaling to the actin cytoskeleton by paxillin during *Drosophila* development. *Mol. Cell. Biol.* 25:979–987.

Chew, T.L., R.A. Masaracchia, Z.M. Goeckeler, and R.B. Wysolmerski. 1998. Phosphorylation of non-muscle myosin II regulatory light chain by p21-activated kinase (gamma-PAK). *J. Muscle Res. Cell Motil.* 19:839–854.

Chrzanowska-Wodnicka, M., and K. Burridge. 1996. Rho-stimulated contractility drives the formation of stress fibers and focal adhesions. *J. Cell Biol.* 133:1403–1415.

Couchman, J.R., and D.A. Rees. 1979. The behaviour of fibroblasts migrating from chick heart explants: changes in adhesion, locomotion and growth, and in the distribution of actomyosin and fibronectin. *J. Cell Sci.* 39:149–165.

Crowley, E., and A. Horwitz. 1995. Tyrosine phosphorylation and cytoskeletal tension regulate the release of fibroblast adhesions. *J. Cell Biol.* 131:525–537.

Edwards, D.C., L.C. Sanders, G.M. Bokoch, and G.N. Gill. 1999. Activation of LIM-kinase by Pak1 couples Rac/Cdc42 GTPase signalling to actin cytoskeletal dynamics. *Nat. Cell Biol.* 1:253–259.

Hashimoto, S., A. Tsubouchi, Y. Mazaki, and H. Sabe. 2001. Interaction of paxillin with p21-activated kinase (PAK). Association of paxillin alpha with the kinase-inactive and the Cdc42-activated forms of PAK3. *J. Biol. Chem.* 276:6037–6045.

Heiple, J.M., S.D. Wright, N.S. Allen, and S.C. Silverstein. 1990. Macrophages form circular zones of very close apposition to IgG-coated surfaces. *Cell Motil. Cytoskeleton.* 15:260–270.

Hinz, B., W. Alt, C. Johnen, V. Herzog, and H.W. Kaiser. 1999. Quantifying lamella dynamics of cultured cells by SACED, a new computer-assisted motion analysis. *Exp. Cell Res.* 251:234–243.

Ishibe, S., D. Joly, X. Zhu, and L.G. Cantley. 2003. Phosphorylation-dependent paxillin-ERK association mediates hepatocyte growth factor-stimulated epithelial morphogenesis. *Mol. Cell.* 12:1275–1285.

Ito, A., T.R. Kataoka, M. Watanabe, K. Nishiyama, Y. Mazaki, H. Sabe, Y. Kitamura, and H. Nojima. 2000. A truncated isoform of the PP2A B56 subunit promotes cell motility through paxillin phosphorylation. *EMBO J.* 19:562–571.

Koh, C.G., E. Manser, Z.S. Zhao, C.P. Ng, and L. Lim. 2001. Beta1PIX, the PAK-interacting exchange factor, requires localization via a coiled-coil region to promote microvillus-like structures and membrane ruffles. *J. Cell Sci.* 114:4239–4251.

Kovacs, M., J. Toth, C. Hetenyi, A. Malnasi-Csizmadia, and J.R. Sellers. 2004. Mechanism of blebbistatin inhibition of myosin II. *J. Biol. Chem.* 279:35557–35563.

Kraynov, V.S., C. Chamberlain, G.M. Bokoch, M.A. Schwartz, S. Slabaugh, and K.M. Hahn. 2000. Localized Rac activation dynamics visualized in living cells. *Science.* 290:333–337.

Laukaitis, C., D. Webb, K. Donais, and A. Horwitz. 2001. Differential dynamics of α5 integrin, paxillin, and α-actinin during formation and disassembly of adhesions in migrating cells. *J. Cell Biol.* 153:1427–1440.

Lee, J., and K. Jacobson. 1997. The composition and dynamics of cell-substratum adhesions in locomoting fish keratocytes. *J. Cell Sci.* 110:2833–2844.

Lin, C.H., and P. Forscher. 1995. Growth cone advance is inversely proportional to retrograde F-actin flow. *Neuron.* 14:763–771.

Liu, Z.X., C.F. Yu, C. Nickel, S. Thomas, and L.G. Cantley. 2002. Hepatocyte growth factor induces ERK-dependent paxillin phosphorylation and regulates paxillin-focal adhesion kinase association. *J. Biol. Chem.* 277:10452–10458.

Manabe, R., M. Kovalenko, D.J. Webb, and A.R. Horwitz. 2002. GIT1 functions in a motile, multi-molecular signaling complex that regulates protrusive activity and cell migration. *J. Cell Sci.* 115:1497–1510.

Manser, E., H.Y. Huang, T.H. Loo, X.Q. Chen, J.M. Dong, T. Leung, and L. Lim. 1997. Expression of constitutively active alpha-PAK reveals effects of the kinase on actin and focal complexes. *Mol. Cell. Biol.* 17:1129–1143.

Manser, E., T.H. Loo, C.G. Koh, Z.S. Zhao, X.Q. Chen, L. Tan, I. Tan, T. Leung, and L. Lim. 1998. PAK kinases are directly coupled to the PIX family of nucleotide exchange factors. *Mol. Cell.* 1:183–192.

Mitchison, T., and M. Kirschner. 1988. Cytoskeletal dynamics and nerve growth. *Neuron.* 1:761–772.

Mostafavi-Pour, Z., J.A. Askari, S.J. Parkinson, P.J. Parker, T.T. Ng, and M.J. Humphries. 2003. Integrin-specific signaling pathways controlling focal adhesion formation and cell migration. *J. Cell Biol.* 161:155–167.

Nishiya, N., W.B. Kiosses, J. Han, and M.H. Ginsberg. 2005. An alpha4 integrin-paxillin-Arf-GAP complex restricts Rac activation to the leading edge of migrating cells. *Nat. Cell Biol.* 7:343–352.

Palecek, S.P., C.E. Schmidt, D.A. Lauffenburger, and A.F. Horwitz. 1996. Integrin dynamics on the tail region of migrating fibroblasts. *J. Cell Sci.* 109:941–952.

Phee, H., R.T. Abraham, and A. Weiss. 2005. Dynamic recruitment of PAK1 to the immunological synapse is mediated by PIX independently of SLP-76 and Vav1. *Nat. Immunol.* 6:608–617.

Ren, X.D., W.B. Kiosses, and M.A. Schwartz. 1999. Regulation of the small GTP-binding protein Rho by cell adhesion and the cytoskeleton. *EMBO J.* 18:578–585.

Ren, X., W. Kiosses, D. Sieg, C. Otey, D. Schlaepfer, and M. Schwartz. 2000. Focal adhesion kinase suppresses Rho activity to promote focal adhesion turnover. *J. Cell Sci.* 113:3673–3678.

Ridley, A.J. 2001. Rho GTPases and cell migration. *J. Cell Sci.* 114:2713–2722.

Romashko, A.A., and M.R. Young. 2004. Protein phosphatase-2A maintains focal adhesion complexes in keratinocytes and the loss of this regulation in squamous cell carcinomas. *Clin. Exp. Metastasis.* 21:371–379.

Sanders, L., F. Matsumura, G. Bokoch, and P. de Lanerolle. 1999. Inhibition of myosin light chain kinase by p21-activated kinase. *Science.* 283:2083–2085.

Schoenwaelder, S., and K. Burridge. 1999. Bidirectional signaling between the cytoskeleton and integrins. *Curr. Opin. Cell Biol.* 11:274–286.

Sells, M.A., A. Pfaff, and J. Chernoff. 2000. Temporal and spatial distribution of activated Pak1 in fibroblasts. *J. Cell Biol.* 151:1449–1458.

Tuazon, P.T., W.C. Spanos, E.L. Gump, C.A. Monnig, and J.A. Traugh. 1997. Determinants for substrate phosphorylation by p21-activated protein kinase (gamma-PAK). *Biochemistry.* 36:16059–16064.

Turner, C.E. 2000. Paxillin and focal adhesion signalling. *Nat. Cell Biol.* 2:E231–E236.

Webb, D.J., K. Donais, L.A. Whitmore, S.M. Thomas, C.E. Turner, J.T. Parsons, and A.F. Horwitz. 2004. FAK-Src signalling through paxillin, ERK and MLCK regulates adhesion disassembly. *Nat. Cell Biol.* 6:154–161.

Webb, D.J., M.J. Schroeder, C.J. Brame, L. Whitmore, J. Shabanowitz, D.F. Hunt, and A.R. Horwitz. 2005. Paxillin phosphorylation sites mapped by mass spectrometry. *J. Cell Sci.* 118:4925–4929.

West, K.A., H. Zhang, M.C. Brown, S.N. Nikolopoulos, M.C. Riedy, A.F. Horwitz, and C.E. Turner. 2001. The LD4 motif of paxillin regulates cell spreading and motility through an interaction with paxillin kinase linker (PKL). *J. Cell Biol.* 154:161–176.

Young, M.R., K. Kolesiak, and J. Meisinger. 2002. Protein phosphatase-2A regulates endothelial cell motility and both the phosphorylation and the stability of focal adhesion complexes. *Int. J. Cancer.* 100:276–282.

Yuruker, B., and V. Niggli. 1992. Alpha-actinin and vinculin in human neutrophils: reorganization during adhesion and relation to the actin network. *J. Cell Sci.* 101:403–414.

Zhang, H., D.J. Webb, H. Asmussen, and A.F. Horwitz. 2003. Synapse formation is regulated by the signaling adaptor GIT1. *J. Cell Biol.* 161:131–142.

Zhang, H., D.J. Webb, H. Asmussen, S. Niu, and A.F. Horwitz. 2005. A GIT1/PIX/Rac/PAK signaling module regulates spine morphogenesis and synapse formation through MLC. *J. Neurosci.* 25:3379–3388.

Zhao, Z.S., E. Manser, T.H. Loo, and L. Lim. 2000. Coupling of PAK-interacting exchange factor PIX to GIT1 promotes focal complex disassembly. *Mol. Cell. Biol.* 20:6354–6363.